Centennial-to-millennial-scale periodicities of Holocene climate and sediment injections off the western Barents shelf, 75°N

M. SARNTHEIN, S. VAN KREVELD, H. ERLENKEUSER, P. M. GROOTES, M. KUCERA, U. PFLAUMANN AND M. SCHULZ

BOREAS

Sarnthein, M., van Kreveld, S., Erlenkeuser, H., Grootes, P. M., Kucera, M., Pflaumann, U. & Schulz, M. 2003 (September): Centennial-to-millennial-scale periodicities of Holocene climate and sediment injections off the western Barents shelf, 75°N. *Boreas*, Vol. 32, pp. 447–461. Oslo. ISSN 0300-9483.

At the western continental margin of the Barents Sea, 75°N, hemipelagic sediments provide a record of Holocene climate change with a time resolution of 10–70 years. Planktic foraminifera counts reveal a very early Holocene thermal optimum 10.7–7.7 kyr BP, with summer sea surface temperatures (SST) of 8°C and a much enhanced West Spitsbergen Current. There was a short cooling between 8.8 and 8.2 kyr BP. In the middle and late Holocene summer, SST dropped to 2.5°–5.0°C, indicative of reduced Atlantic heat advection, except for two short warmings near 2.2 and 1.6 kyr BP. Distinct quasi-periodic spikes of coarse sediment fraction (with large portions of lithic grains, benthic and planktic foraminifera) record cascades of cold, dense winter water down the continental slope as a result of enhanced seasonal sea ice formation and storminess on the Barents shelf over the entire Holocene. The spikes primarily cluster near recurrence intervals of 400–650 and 1000–1350 years, when traced over the entire Holocene, but follow significant 885-/840- and 505-/605-year periodicities in the early Holocene. These non-stationary periodicities mimic the Greenland-^{10}Be variability, which is a tracer of solar forcing. Further significant Holocene periodicities of 230, (145) and 93 years come close to the deVries and Gleissberg solar cycles.

Michael Sarnthein (e-mail: ms@gpi.uni-kiel.de) and Shirley van Kreveld, Institut für Geowissenschaften, University of Kiel, D-24098 Kiel, Germany; Helmut Erlenkeuser and Pieter M. Grootes, Leibniz Labor, University of Kiel, D-24098 Kiel, Germany; Michal Kucera, Department of Geology, Royal Holloway University of London, Egham, TW20 0EX, UK; Uwe Pflaumann and Michael Schulz, Institut für Geowissenschaften, University of Kiel, D-24098 Kiel, Germany; *received 2nd September 2002, accepted 17th February 2003.*

On the basis of relative isotope temperature stability on the Greenland summit, the Holocene climate is considered to be fairly stable on centennial and longer time scales compared to glacial climates, which underwent extreme temperature changes within decades along with the 1500-year Dansgaard Oeschger (DO) cycles (Dansgaard *et al.* 1993; Grootes & Stuiver 1997), as long as sea level was lowered by more than 45 m (Schulz *et al.* 1999).

Nevertheless, significant climatic variations also occurred during most of the Holocene. In the North Atlantic realm, climatic variations are recorded by glacier advances and tree-line changes in Scandinavia (e.g. Karlén 1993; Dahl & Nesje 1996; summary in Huntley *et al.* 2002) and in the Alps (Patzelt 1999), as well as by fluctuations in lake level and net precipitation in Sweden (Harrison & Digerfeldt 1993; Digerfeldt 1998). In particular, sea surface temperatures (SST) varied by up to 4°C in the Norwegian–Greenland Sea and North Atlantic (Koç *et al.* 1993; E. Jansen, pers. comm. 2001 on sediment record MD95-2011), likewise subsurface penetrations of Atlantic water into the Arctic Ocean (Duplessy *et al.* 2001; Hald *et al.* 1999; Lubinski *et al.* 1996, 2001). The isotopic and chemical signatures in the Greenland ice and at the Greenland margin show analogous fluctuations over the Holocene, although at much lower amplitudes (Willemse & Tørnquist 1999; Mayewski *et al.* 1997; Grootes & Stuiver 1997; Schulz & Paul 2002).

Moreover, evidence is ever increasing that millennial-scale cyclicities also persisted during Holocene times, although with generally weaker amplitudes than during glacial times and with the dominant periods still under discussion. Denton & Stuiver (1969) first noted glaciers in northeastern Canada, which fluctuated at 2–3 kyr intervals. Bond *et al.* (1997, 1999) reported cycles in ice-rafting and SST, averaging 1000–2000 years over the entire Holocene, but only 600–1000 years in the early Holocene (Bond *et al.* 1997: fig. 2). Bianchi & McCave (1999) even inferred actual 1500-year DO-style fluctuations in the strength of the flow of North Atlantic Deep Water (NADW). On the other hand, Schulz & Paul (2002) extracted a highly significant and dominant but non-stationary 890-year periodicity from the Holocene GISP2 δ^{18}O (temperature) signal, a period which they ascribe to an internal oscillation of North Atlantic thermohaline circulation (THC). Similar frequencies were deduced for Holocene glacial advances in the Alps (Patzelt 1999) and for Δ^{14}C and ^{10}Be variations as measured in tree rings and GISP2, respectively (Friedrich *et al.* 1999; Bond *et al.* 2001). These data also serve as support for direct solar forcing.

The high-latitude Norwegian Sea and Barents shelf may play an important role in intensifying and documenting the climate signals linked to any forcing, since they occupy a key position in the global system of THC. On the floor of the Barents shelf, near to the polar front, abundant dense winter water is formed by brine-

Taylor & Francis
Taylor & Francis Group

DOI 10.1080/03009480310003351

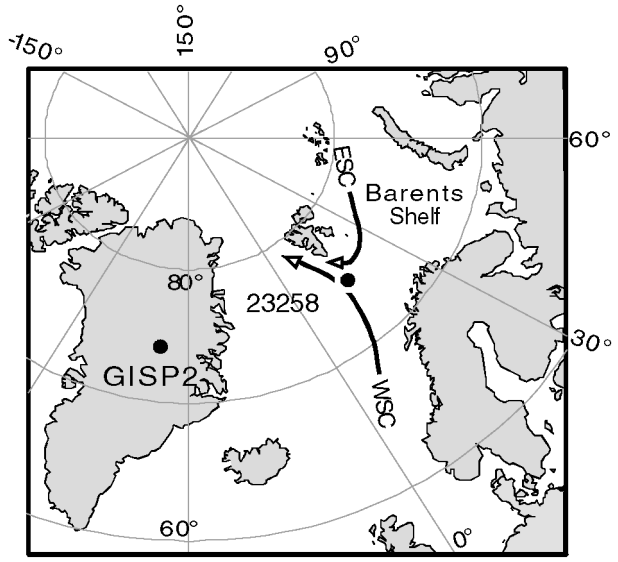

Fig. 1. Location of Site 23258 in the northern Norwegian Sea and of GISP2 ice core in Greenland. WSC = West Spitsbergen Current, ESC = East Spitsbergen Current.

water rejection in the course of seasonal sea-ice production (Backhaus *et al.* 1997; Rumohr *et al.* 2001). This dense water cascades downslope into the Arctic and Nordic Seas, where it contributes to the formation of bottom water, thus intensifying the Atlantic THC. Furthermore, both major fall/winter storms and the cascades of winter water stir up great sediment plumes on the shelf and upper slope. These sediments are carried far downslope in the nepheloid layer and accumulate along the continental apron (Blaume 1992). The outlined mechanism is expected to provide a clear and high-resolution sediment record of past variations in storminess and sea-ice formation near the polar front.

In this article we document long- and short-term changes in ocean climate in the northeastern Norwegian Sea over the past 11.6 kyr; in particular, we infer changes in poleward heat flux in the West Spitsbergen Current at 75°N, on the basis of a sediment record with decadal-to-multidecadal resolution. Special attention is paid to centennial-to-millennial-scale changes in storminess and the extent of sea-ice formation near the polar front. Both processes are expected to provide a sediment signal essentially different from that produced by the plankton inhabiting the warm West Spitsbergen Current.

Material and methods

Kasten core 23258-2 (75°N, 14°E; 1768 m water depth) was retrieved from the northeastern Norwegian Sea at the lower Barents continental slope (Fig. 1) during METEOR cruise 7/2 in 1988 (Hirschleber *et al.* 1988). The continuous and turbidite-free, hemipelagic sediment section between 25 and 415 cm was continuously sampled every single centimetre. Since the top 25-cm section in core 23258-2 was lost by flowing out, we assembled a complete core top section by splicing in the 40-cm-long sediment profile of neighbour (spade) box core 23258-3 (Fig. 2 top; 14 cm in box core '−3' is approximately equivalent to 25 cm in kasten core '−2').

The samples were weighed, freeze-dried, reweighed, wet-sieved through a 63-μm mesh screen and then dry-sieved at 150 μm. The fraction >150 μm was repeatedly split until enough specimens remained to identify and count between 400 and 1000 specimens of planktic foraminifera and the proportion of lithic grains. The high specimen numbers served to cope with the statistical problem of almost monospecific samples from subpolar and polar regions, where *Neogloboquadrina pachyderma* (sin.) accounts for up to 90–100% of the total planktic fauna.

Stable O and C isotopes were analysed on samples of >30 tests of *N. pachyderma* (sin.), 150–250 μm, and 1–10 specimens of the epibenthic species *Cibicidoides wuellerstorfi* (300–415 μm, few samples 250–415 μm). The tests were treated with 99.8% ethanol, cracked and treated with ultrasound in deionized water. The samples were converted to CO_2 with H_3PO_4 in the automated Carbo-Kiel preparation line. The released CO_2 gas was measured online using a Finnigan MAT-251 mass spectrometer at the Leibniz Laboratory of the University of Kiel. The analytical precision of the internal carbonate standard (Solnhofen Limestone), which was run every 10 samples, was 0.07‰ for $\delta^{18}O$ and 0.05‰ for $\delta^{13}C$. The isotope values were calibrated to the Pee Dee Belemnite (PDB) scale using NBS 20.

Seasonal SST variations at 10-m water depth were estimated from planktic foraminifera census counts using the SIMMAX transfer function (Pflaumann *et al.* 1996 and in press), which is based on a maximum similarity index of species assemblages in the 10 best analogues combined with geographical distance weighting between analogue samples. This method is most suited for reconstructing SST of the polar 23258 site because of its extensive database of 947 modern analogues including considerable data from high latitudes (Pflaumann *et al.* in press). Accordingly, the estimates of summer SST between 3°C and 8°C can be well reproduced within 0.9°C, and the bias by no-analogue cases is minor ($r^2 = 0.994$ for measured versus estimated SST). Nevertheless, SIMMAX-based estimates below 2°–3°C tend to be 1°–3.5°C overestimations of actual SST, implying a unilateral bias for cold SST extremes. Overestimation of winter temperatures near the cold end, i.e. near the freezing point, does not exceed 1.5°C.

In order to assess the reliability of the SIMMAX-based SST reconstructions, we used the Artificial

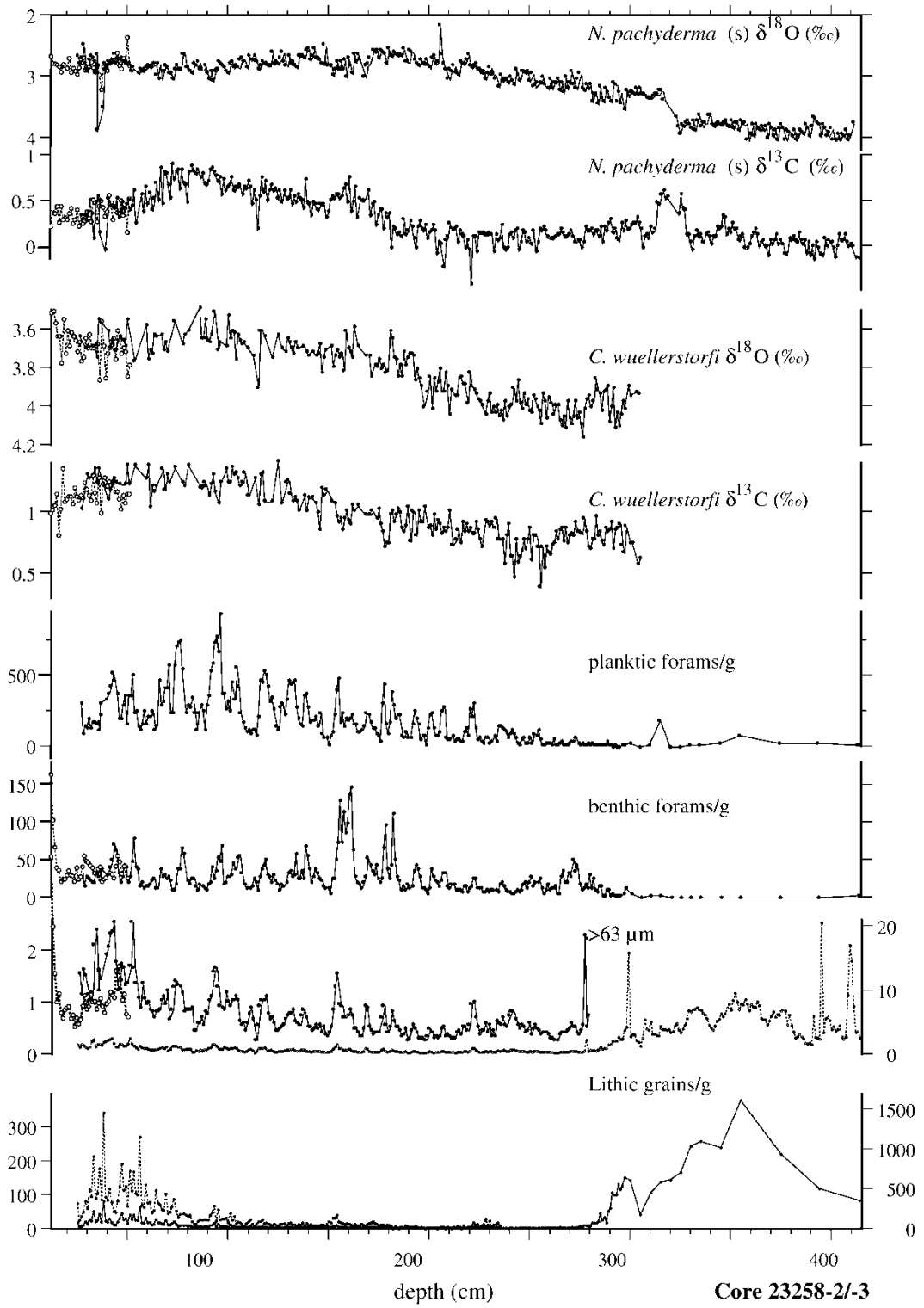

Fig. 2. Planktic and benthic stable isotope records, sediment and grain size composition in spliced cores 23258-2 and -3 (open dots mark records of box core -3) from 0 to 415 cm composite depth below sea floor. δ^{18}O record of *C. wuellerstorfi* in core -3 is corrected for −0.2‰ to account for a systematic analytical offset. Scales of both the grain size record >63 µm in top 280 cm core depth (solid line and open-dot line) and the proportion of lithic grains >150 µm in top 235 cm core depth (dotted line) are enlarged (left-hand scales).

Neural Network (ANN) technique (Malmgren *et al.* 2001), which is based on an algorithm that simulates autonomous learning. Its utility for SST reconstructions has been demonstrated by Malmgren & Nordlund (1997) and Malmgren *et al.* (2001), who also showed that ANN SST reconstructions are independent of SIMMAX. In this study, we developed a new set of ANNs trained on the same 947-sample database with the same summer and winter SST (10 m) definitions as the SIMMAX technique described above. The training followed the procedures outlined in Malmgren *et al.* (2001). We used the Biocomp NGO 2.6 software (maximum of 2 hidden layers with up to 32 neurons; training stopped after 2500 learning epochs or if no improvement occurred after 40 epochs; optimization based on 30 generations with population size of 100; 20% of samples used for test set; fitness based 80% on test set, 20% on training set).

A proxy to produce conservative estimates of the maximum extent of sea ice cover (with >50% sea ice density) in the Nordic Seas was derived from 150 core-top samples (Sarnthein *et al.* in press). They show that SIMMAX-based SST of >2.5°C characterize ice-free conditions during summer, while SST of >0.75°C characterize ice-free conditions during a Little Ice Age- (LIA-) style winter. This approach holds true for almost 100% of all sites seaward of the modern/LIA sea ice margin. On the other hand, many sites seaward of the sea ice also produce SST estimates that are lower than the chosen threshold values. Accordingly, this new SST-based sea ice proxy can only reconstruct the largest possible extent of sea ice in the past. The actual sea ice cover (with an ice density of >50%) was probably more reduced than our reconstructions show.

Twenty-two samples were ^{14}C dated by accelerator mass spectrometry (AMS; Table 1) at the Kiel Leibniz Laboratory (methods in Nadeau *et al.* 1997). Seventeen samples consisted of 623–2668 specimens of *N. pachyderma* (sin.) (150–315 μm; sample weight of 4.3–13.5 mg), picked on relative abundance highs and peaks of this species to minimize the bias of bioturbation. Three samples consisted of low specimen numbers of *N. pachyderma* (dex.) and two dated the organic carbon. In Table 1 all ages are given in ^{14}C kyr, corrected for an average ^{14}C reservoir effect of 400 years; in one case, near the top of Younger Dryas, for 900 years (Bard *et al.* 1994). The ^{14}C ages were finally converted to calendar years BP (Stuiver *et al.* 1998). Reasons for replacing and/or ignoring certain age estimates are given in the discussion section.

Strong and frequent variations in the sediment composition were studied using the spectral analysis program REDFIT (Schulz & Mudelsee 2002), which analyses unevenly spaced time series without prior interpolation.

All data are deposited in the PANGAEA data bank www.pangaea.de.

Results

Oxygen isotope values of *N. pachyderma* (sin.) vary from 2.2‰ to 4.0‰, while carbon isotope values fluctuate from 0.9‰ to 0.4‰ in core 23258 from the northeastern Norwegian Sea (Fig. 2). From 415–325 cm high δ^{18}O values of 4.05–3.7‰ precede an abrupt 0.7‰ decrease at 325–318 cm ascribed to the top of the Younger Dryas. Here the planktic δ^{13}C values show a marked excursion from approximately 0.1‰ to 0.5‰ at 330–312 cm, interpreted as ventilation pulse. From 200 cm to 100 cm depth there follows a gradual δ^{13}C rise and from 70–50 cm depth a final δ^{13}C decrease to the present 0.3/0.5‰ level.

Epibenthic *C. wuellerstorfi* is absent below 305 cm, that is below the planktic δ^{18}O jump at 318–327 cm marking the top of the Younger Dryas (Fig. 2). Further upcore, from 305–220 cm, that is within the earliest Holocene, the δ^{18}O values of *C. wuellerstorfi* remain near 4.0–4.2‰. This level is still characteristic of the Younger Dryas as uniformly recorded in single-grain isotope data obtained from various cores from similar water depths in the Nordic Seas (Vogelsang 1990; Voelker 1999). In the top 220 cm section the values gradually decrease to 3.5‰, 100 cm above the planktic δ^{18}O shift. Benthic δ^{13}C values also change from a low average of 0.6–0.8‰ at more than 230 cm to high values of 1.1–1.4‰ in the top 150 cm depth, which are characteristic of the modern deep water formed in the Nordic Seas (Weinelt *et al.* 2001).

The coarse fraction >63 μm in the bulk sediment varies from 0% to 22%. There is a series of distinct peaks, however, that do not exceed 3% in the top 280 cm of the core (Fig. 2). Most match the maxima in planktic and benthic foraminifera concentrations.

In the coarse fraction, lithic grains consist mostly of colourless, transparent quartz and sediment clasts, with moderate to low amounts of hematite-stained quartz, feldspar (occasionally hematite-coated), brown glass, volcanic rock fragments, crystalline grains and detrital carbonate. The lithic grain concentration varies from 0 to 1615 grains >150 μm per gram dry sediment, with a broad maximum during the (cold) interval 415–310 cm. Concentrations are low from 280–80 cm, but increase slightly from 80 cm to the top, in parallel with the coarse fraction >63 μm and with decreasing planktic δ^{13}C values (Fig. 2).

The planktic foraminifera fauna in core 23258-2 consists of polar, subpolar and cosmopolitan species (Fig. 3), today also identified in nearby sediment traps (Jensen 1998). The fauna is dominated by the polar *N. pachyderma* (sin.) (100–16%) and the subpolar *Turborotalita quinqueloba* (65–0%). The subpolar species *N. pachyderma* (dex.) and *Globigerina bulloides* vary from 23% to 0% and from 17% to 0%, respectively. The cosmopolitan *Globigerinita glutinata* varies from 1% to 0%. The concentrations of planktic and benthic foraminifera oscillate between 0 and 920 and 0 and 145

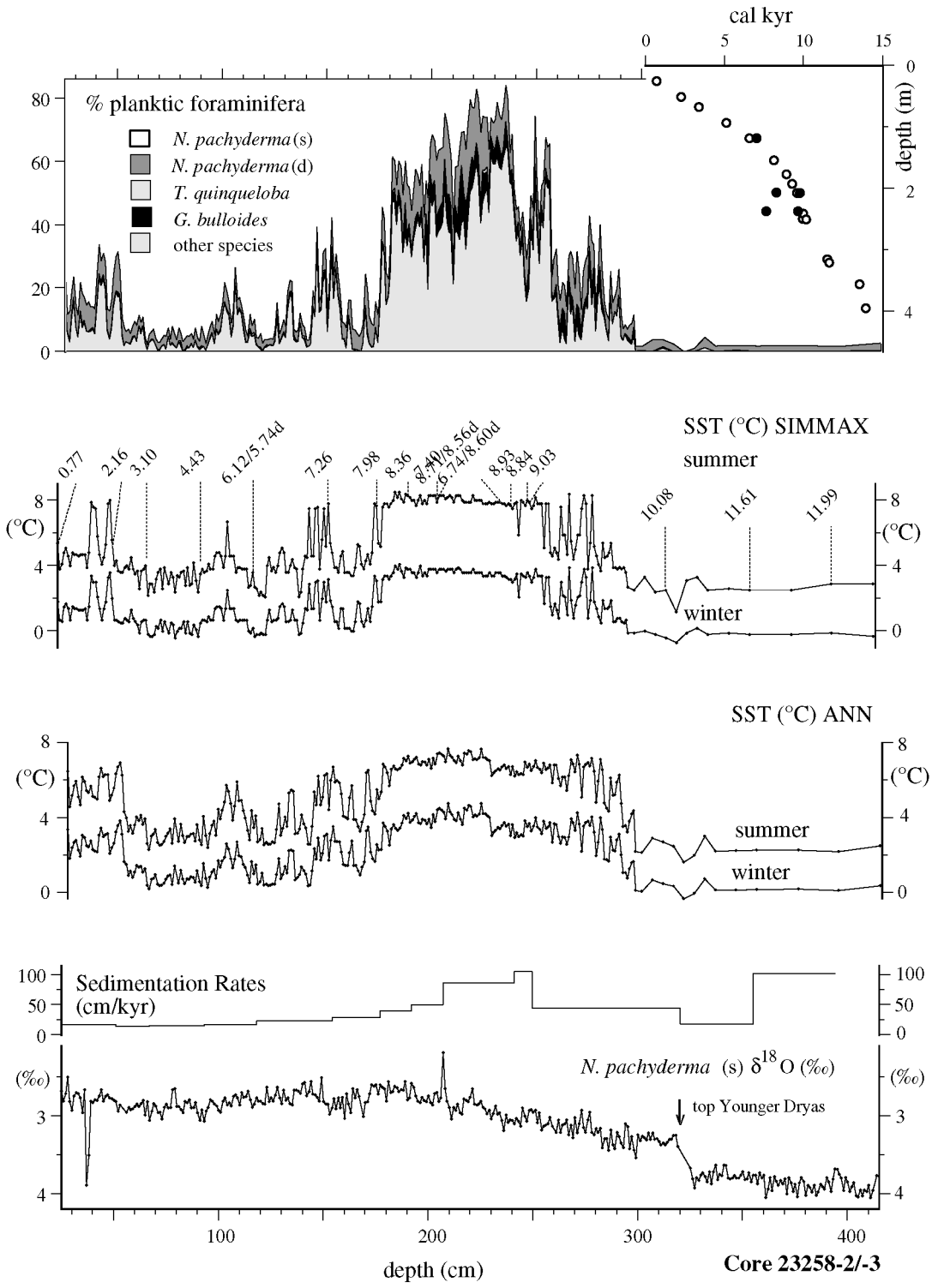

Fig. 3. Composition of planktic foraminifera assemblage, SIMMAX- and ANN-based sea surface temperature records for winter and summer, with ^{14}C datings on right coiled (d) and left coiled (no specification) specimens of *N. pachyderma* (Table 1); age-depth plot (full dots are outlier dates of *N. pachyderma* sinistral and dextral, not used in the age model) and sedimentation rates in core 23258-2 versus planktic $\delta^{18}O$ record.

Table 1. ^{14}C dates and other age control points in sediment core 23258/2 and /3.

Lab. no.	Core	Depth (cm)	*N. pachyderma*	AMS ^{14}C age −400 yr res. corr. (years)	1 error (+/− years)	cal. age BP (years)	Time res. at 1-cm sampling (years)	Remarks
Age control points								
KIA9191	Box core 23258-3	17	Sinistral	780	35	712		
KIA9192	23258-3	36	Sinistral	1785	30	1781	56	
KIA7648	Kasten core 23258-2	25	Sinistral	765	35	698		
KIA7649	23258-2	51	Sinistral	2155	30	2244	60	
KIA7650	23258-2	67	Sinistral	3100	35	3376	71	
KIA7651	23258-2	93	Sinistral	4425	40	5110	67	
KIA11534	23258-2	118	Dextral	5740	70	6567	58	
KIA7653	23258-2	154	Sinistral	7260	45	8106	43	
KIA7654	23258-2	177	Sinistral	7980	45	8892	34	
KIA8553	23258-2	192	Sinistral	8360	40	9271	25	
KIA11535	23258-2	207	Dextral	8555	55	9570	20	
KIA9193	23258-2	241	Sinistral	8930	70	9965	12	
	23258-2	249.5	Sinistral			10046	10	Average of ^{14}C ages at 249 and 250 cm depth
KIA7657	23258-2	315	Sinistral	10080	70	11490	22	^{14}C res. corr. 900 yrs (Bard *et al.* 1994)
		320				11600	22	Age correlated to GISP2 age of top Younger Dryas
KIA7658	23258-2	355	Sinistral	11610	55	13530	55	
KIA7659	23258-2	394	Sinistral	11990	60	13911	10	
Two datings averaged at 249.5 cm depth								
KIA8554	23258-2	249	Sinistral	8835	50	9937		
KIA9354	23258-2	250	Sinistral	9035	55	10155		
Datings not used in age model (see black dots in Fig. 3)								
KIA7652	23258-2	118	Sinistral	6120	40	7019		Replaced by age of *N. pachyderma* dextral
KIA7655	23258-2	206	Sinistral	7400	40	8264		Ignored because of age reversal
KIA9353	23258-2	207	Sinistral	8710	50	9742		Replaced by age of *N. pachyderma* dextral
KIA7656	23258-2	237	Sinistral	6740	50/−45	7607		Replaced by age of *N. pachyderma* dextral
KIA11536	23258-2	237	Dextral	8600	70	9630		Ignored because of age reversal

specimens per gram dry sediment, respectively. Common distinct maxima of both planktic and benthic foraminifera occur at approximately 20-cm intervals in the top 255 cm. Benthic and planktic foraminifera are rare to absent during the lithic-grain maximum at 415–310 cm.

SIMMAX-based summer SST estimates from planktic foraminifera range near 2.5°C below 300 cm and rise to approximately 8°C from 260 to 180 cm (Fig. 3). Subsequent summer SST dropped to 2.5–5.0°C in the top 180 cm, with a few extremely narrow warm intervals of about 7.5°C near 150 and 50–40 cm. Winter temperatures are approximately 3–4°C lower than during summer. Our SIMMAX-based SST reconstruction is largely corroborated by the ANN estimates. The main difference between the two techniques is that the ANN-based record shows slightly more short-term variability, somewhat warmer SST near 5000 and during the last 1000 years (Fig. 3).

Discussion

Age model

The age model is based mainly on ^{14}C dating. In addition, the abrupt planktic δ^{18}O decrease at 325–318 cm depth is used as prominent age control point, being tied to the end of the Younger Dryas at 11.6 cal. kyr BP in the GISP2 δ^{18}O air temperature record, the base of the Holocene. Within the Holocene, the age model is based on linear interpolation between ^{14}C dates calibrated to calendar years (Fig. 3, upper right). The resulting sedimentation rates gradually decrease from $>$100 cm/kyr in the Early Holocene to approximately 15 cm/kyr in the middle and late Holocene (Fig. 3), yielding an average sampling resolution of $<$10–70 years (Table 1).

Near to the Barents shelf and slope, the AMS ^{14}C ages and the resulting age model may be biased by unusually high, intermittent downslope injections of subfossil specimens of *N. pachyderma* (sin.) and organic matter reworked within the nepheloid layer (Rumohr *et al.* 2001). For example, the Holocene AMS ^{14}C dates show various major and minor age reversals. Moreover, two ^{14}C ages measured on total organic carbon at 160–165 cm (11.38 ^{14}C kyr BP) and 189–194 cm (14.59 ^{14}C kyr BP) (Blaume 1992; not listed in Table 1) are much older than the ambient foraminifera-based dates.

To constrain the potential age bias resulting from reworked old tests of *N. pachyderma* (sin.), we ^{14}C-dated three *N. pachyderma* (dex.) samples. Extremely low specimen numbers unfortunately prevented us from dating more samples of this species. Its specimens can only derive from the local pelagial in the warm West Spitsbergen Current on top of core site 23258, but barely from lateral sediment input from the polar Barents shelf, different from tests of *N. pachyderma* (sin.). Two of three paired ^{14}C ages show that age estimates based on *N. pachyderma* (dex.) are only 150–400 years younger than those based on *N. pachyderma* (sin.), which were therefore ignored in our age model. The age difference corresponds to a proportion of 5–10% of reworked *N. pachyderma* (sin.) tests, which were formed after the Bølling time transgression, with an assumed average age of 11 500 years BP. However, the paired age estimates also show that the influence of reworked old specimens on the ^{14}C ages of *N. pachyderma* (sin.) is generally so low that it can almost be neglected.

We also ignored an age of *N. pachyderma* (dex.) at 237 cm depth (8600 y $\pm$ 70 = 9630 cal. yr BP) because it would imply an aberrant sedimentation rate of 250–∞ cm/kyr compared to a neighbour ^{14}C age of *N. pachyderma* (dex.) at 207 cm depth (8555 y $\pm$ 55 = 9570 cal. yr BP), 30 cm further upcore. However, no pertinent sediment structures such as graded and/or coarse-grained sediment layers occur in this depth range, which might record such an extreme and 'instantaneous' sediment accumulation. For this reason, an interpolated age of 9921 cal. yr was derived for 237 cm depth from the average sedimentation rate of 91.14 cm/ kyr, characteristic of the Early Holocene section.

The resulting age model (Table 1, Fig. 3) produces Early Holocene sediment records, where both a significant increase in coarse fraction near 155–175 cm depth and the final phase of a major cooling indeed are consistent with the prominent '8,200-yr cooling' (8330 $\pm$ 80 yr BP according to Baldini *et al.* 2002) and its precursor cooling trend found in the Greenland δ^{18}O records (Grootes & Stuiver 1997; Johnsen *et al.* 2001).

Long-term change in Holocene sea surface conditions

The SIMMAX-based and ANN-based SST records reveal three different climatic regimes of unequal length in the Holocene at Site 23258 (Figs 3, 4). The initial δ^{18}O decrease by 0.7‰ between 11.9 and 11.6 kyr ago was just paralleled by a slight SIMMAX-based and ANN-based cooling and thus indicates primarily a global ice volume decrease and/or a local meltwater injection. The subsequent Preboreal SST rise lasted for $<$1000 years 11.6–10.75 kyr ago and included 3 stepwise massive warmings accumulating to a total of 7°C for summer. They indicate a rapid poleward advance of the warm West Spitsbergen Current. On the basis of threshold SST estimates (Sarnthein *et al.* in press) sea ice of $>$50% concentration disappeared during both summer and winter near 11.25 kyr BP, a prelude to the Holocene thermal maximum. During that time coarse, lithic grains characteristic of ice-rafted debris (IRD) and other local lateral sediment input disappeared almost completely (Fig. 4).

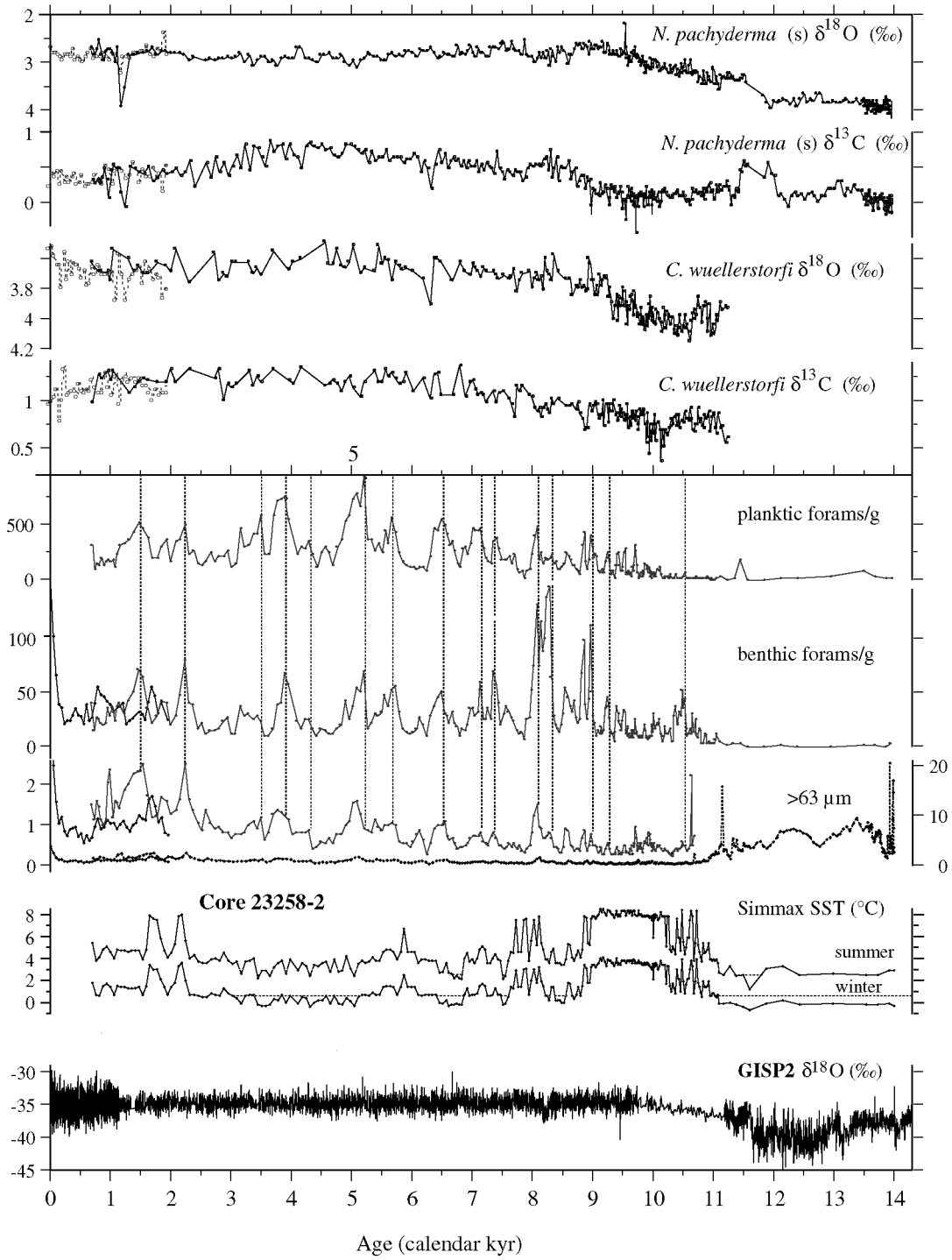

Fig. 4. Planktic and benthic stable isotopes, sediment composition, grain sizes, seasonal sea surface temperatures (SST), >50% sea ice cover during summer and winter (horizontal dotted lines), and GISP2 δ^{18}O record (Grootes & Stuiver 1997) versus age.

High SST of 7.5–8.5°C during summer characterize the second major Holocene unit. This thermal optimum appears at Site 23258, 75°N, as early as 10.75–8.8/7.7 kyr BP (Fig. 4). During this time, the ANN-based SST record displays a SST variability that is little higher than the SIMMAX-based record (Fig. 3), the SST variations of which are smoothed by using 10 modern-analogue samples. This thermal maximum is

almost coeval with a SST maximum in the western Fram Strait (Bauch *et al.* 2001) and the prominent maximum of thermophilous molluscs on Spitsbergen (Salvigsen *et al.* 1992). However, it is much earlier than the thermal maximum in the mid-latitude Atlantic (Marchal *et al.* 2002) and a recent chironomid record from northern Fennoscandia (Korholla *et al.* 2002). It is coeval with the Early Holocene insolation maximum and mimics the climate trends recorded in Greenland and Severnaya Zemlya ice cores (10.5/9.5–8.5 kyr BP; Koerner & Fisher 1990; Alley *et al.* 1999; Lubinski *et al.* 1999). Both high SST and low planktic δ^{13}C values (0–0.25‰ corresponding to 0.8–1.1‰ in Dissolved Inorganic Carbon (DIC) of ambient sea water (Labeyrie & Duplessy 1985) reflect a maximum advection of warm, but poorly ventilated Atlantic surface water (Sarnthein *et al.* 1995; Simstich 1999) in the West Spitsbergen Current from 10.7 to 8.8 kyr BP (Figs 1, 4). The intensified warm-water advection also implied a high flux of pelagic carbonate (Weinelt *et al.* 2001), thus leading to maximum sedimentation rates (Fig. 3). Near the beginning and end of the thermal optimum the SST records appear highly unstable and flickering within decades to centuries. So far, we do not know whether this is a real signal or an artifact because of lateral sediment injections (see below).

The 3000-year-long Holocene optimum was interrupted by an apparently 600-year-long significant cooling down to 3–5°C during summer, dated to 8.8–8.2 kyr ago for SIMMAX SST (Fig. 4) and to 8.55–8.2 for ANN SST. This cold event corresponds to the well-known cold spell in the Greenland ice cores (Johnsen *et al.* 2001) and various marine (De Vernal *et al.* 1997; Wang *et al.* 1999; Bond *et al.* 2001) and terrestrial (von Grafenstein *et al.* 1998; Baldini *et al.* 2002) sediment records, a cold spell culminating near 8300 yr BP. The onset, middle and end of the cold spell are marked by maxima in coarse fraction, as we surmise, the result of lateral sediment discharge tied to either storminess or sea-ice-induced formation of winter water cascades from the Barents shelf, in harmony with the formation of winter sea ice depicted in Fig. 4. The reworked polar-foraminifera specimens were obviously insufficient to produce a prolongation of the cold spell by more than 50–100 years.

The overall cooling trend after 9 kyr BP may resemble a response to decreasing insolation during summer, per analogy to other published records (Koerner & Fisher 1990; Alley *et al.* 1999). Within this time, the last 7700 years form the third distinct and longest unit of the Holocene. It began with a sudden and almost irreversible SST reduction of 3°C, coeval with cold event b′ in a speleothem δ^{18}O record from Ireland and in GISP2 (McDermott *et al.* 2001). Later on, SST varied between 2°C and 5°C during summer. Winter SST generally dropped to 1°C and less, leading to extensive periods of winter sea ice. Some centuries possibly had a perennial sea ice cover, such as near 6.75 kyr BP. During this time the intensity of heat advection with the warm West Spitsbergen Current was reduced. In contrast, the polar East Spitsbergen Current (ESC) and/or the wake of the Jan Mayen Current which are both marked by high planktic δ^{13}C values of 0.7–0.8‰ (equal to 1.5–1.65‰ of DIC in ambient sea water) advanced closer to Site 23258 and the local polar front located along the southern margin of the ESC shifted south.

The generally cool Late Holocene was interrupted by some short-lasting, but marked warmings. During summer they reached 7–8°C around 5500, 2200 and 1800–1600 years ago. The latter two 'M-shaped' excursions are also known from North GRIP (Johnsen *et al.* 2001), approximately coeval with the Roman climatic optimum, from core MD95-2011 from the Voering Plateau (Marchal *et al.* 2002), and from the Irish speleothem record (McDermott *et al.* 2001). These short-term warmings were superimposed on two more extended phases of general slight warming and disappearing sea ice from 6.4–5.2 and 3.0–1.6 kyr BP. The Late Holocene warming is more pronounced in the ANN-based record. The underlying increase in Atlantic warm-water advection also induced a general drop in planktic δ^{13}C at Site 23258 to 0.0–0.5‰ (Fig. 4), characteristic of Atlantic inflow water (Sarnthein *et al.* 1995; Simstich 1999). Marchal *et al.* (2002) showed similar trends of Late Holocene warming in planktic foraminifera-based records of summer SST on the Voering Plateau and in the eastern Irminger Sea. Like the SST curves at Site 23258, these records stem from the main track of North Atlantic poleward heat advection and hence support our view of a slight Late Holocene increase in thermohaline circulation. During this time a significant warming was also recorded from northern Fennoscandia (Korholla *et al.* 2002).

In contrast to SST, the Holocene planktic δ^{18}O values remained almost constant (Fig. 4) except for a minor δ^{18}O increase during the cold period 8.6–8.2 kyr BP and a unique short-term planktic δ^{18}O maximum at the start of the Dark-Age Cold Period (1600–1000 yr BP; McDermott *et al.* 2001). The planktic δ^{18}O curve appears largely uncoupled from SST variations throughout the Holocene. In part, this may be linked to a significant portion of polar *N. pachyderma* (sin.) specimens that were laterally admixed downslope from the cold Barents shelf water, as discussed below. More important, the δ^{18}O signal of *N. pachyderma* (sin.) is formed at 70–200 m water depth (Simstich *et al.* 2002), whereas SIMMAX-based and ANN-based SST estimates are calibrated to 10 m depth. Accordingly, we surmise that the Holocene warmings of the West Spitsbergen Current were largely confined to a thin veneer of surface water on top of the calcification habitat of *N. pachyderma* (sin.).

Lateral sediment injections

As outlined, Holocene sediments of the last 11.1 kyr are barren of IRD, in harmony with absent major iceberg sources in the Holocene Nordic Seas. However, there are some 13–15 discrete sediment layers enriched in coarse fraction, which are non-graded and not separated by basal unconformities, thus non-turbiditic. Most coarse-fraction maxima comprise similar excursions in the abundance of planktic and benthic foraminifera and likewise, of lithic grains in the 63–150-μm fraction (Figs 2, 4). The coeval excursions of such different sediment components may help to trace down the origin of the layers at Site 23258 to lateral sediment injections which form the most spectacular signals of Holocene climate variability (Fig. 4), in harmony with modern oceanographic findings and sediment trap data (Backhaus *et al.* 1997; Rumohr *et al.* 2001).

The trap data reveal a massive downslope transport of sediment from the Barents shelf. This conclusion is based on (1) a general increase in the fluxes of carbonate and particulate organic carbon with increasing water depth (Thomsen *et al.* 2001); (2) a clear maximum in the lithogenic and carbonate flux during fall and winter (Honjo 1990), which suggests a link between sediment transport and cascades of dense winter water from the Barents shelf; and (3) tests of benthic foraminifera, found as far as 350 m above the sea floor (von Bodungen *et al.* 1991).

A series of near-bottom T-S records on the slope near Site 23258 (Blaume 1992) shows that plenty of dense bottom water is produced along with sea ice-induced brine formation close to the study area at 75°50 N, 114°53 E and 0–363 m water depth (Midtun 1985; Backhaus *et al.* 1997). The resulting bottom currents are sufficient to erode sediment on the nearby Barents shelf and upper continental slope. The ensuing sediment plumes today penetrate down to a major pycnocline near 1200 m water depth, from where the coarse particles fall out to Site 23258.

Common extreme fall and winter storms on the Barents shelf form an alternative powerful mechanism that leads to extensive sediment reworking on the shelf and the formation of sediment plumes, as found in front of the Kveitehola valley (Rumohr *et al.* 2001; Fohrmann *et al.* 2001).

Relative to the planktic δ^{18}O record the injections of reworked benthic foraminifera resulted in an apparent delay of the benthic δ^{18}O signal of *C. wuellerstorfi* in the Early Holocene, where Younger Dryas-style high values of 3.95–4.15‰ persisted until 9800 cal. yr BP (230 cm depth; for comparison, the δ^{18}O level of glacial Norwegian Sea Overflow water was 4.2–4.9‰). Only over the last 9200 yr BP (top 190 cm core depth) did the benthic δ^{18}O values reach 3.5–3.7‰, characteristic of the Holocene, as corroborated by high benthic δ^{13}C values of 1.2–1.6‰ (Fig. 4).

In summary, the discrete layers of coarser grained deposits form a striking document of short-term increased lateral sediment injections. They form distinct signals of climate deterioration which probably involved periods of both cascades of dense brine water induced by seasonal sea ice formation and/or enhanced storminess on the Barents shelf south of Svalbard. Accordingly, the Early Holocene thermal maximum was almost free of sediment injections, whereas prominent sediment injections mark the onset and end of the cold spell 8800–8200 years ago (Fig. 4). The injection record of the last 8000 years mimics with great detail a series of short periods with predominantly stormy ocean climate deduced from raised-beach ridges along the northern coastline of Kola Peninsula (Møller *et al.* 2002). This match suggests similar oscillations of storminess over the broad region of the Barents shelf. Moreover, the injections are coeval with harsher climates on Greenland (Johnsen *et al.* 2001: fig. 8) and, accordingly, with a reduced poleward heat transfer from the subtropical Atlantic, although the relationship to short-term, small-scale local SST variations is not unequivocal (Fig. 4).

Frequency of downslope sediment injections

To constrain the ultimate climate forcing which may induce the numerous events of Holocene cooling and downslope sediment injections at Site 23258, we estimated the most prominent concentrations of variability in the spectral domain. Over the entire Holocene, the recurrence intervals of benthic/planktic foraminifera and the total coarse fraction are non-stationary and primarily cluster within two bands, i.e. between 400 and 650 years and between 1000 and 1350 years (Fig. 5, right panel). From 10 to 6 kyr BP the variance of planktic and benthic foraminifera and the coarse fraction is centred at significant (>80%) spectral peaks near 885, 505 (in one case), 230, 145 and 93 years (Fig. 5, left panel).

The latter periodicities are distinctly shorter than the DO cycles in marine isotope stages (MIS) 2–4, but possibly correspond to the Holocene spacings of red-stained IRD quartz spikes in the North Atlantic (Bond *et al.* 2001) and of percent *Globigerina quinqueloba* in the Norwegian Channel (Klitgaard-Kristensen *et al.* 2001). In the better resolved Early Holocene record, these fluctuations reveal a dominant periodicity of 850–900 years similar to the Early Holocene sediment injections at Site 23258.

The potential origin of the maxima in spectral power density and the event spacings seen in core 23258 may perhaps be constrained through their similarity with variations of cosmogenic ^{14}C and ^{10}Be isotopes (Beer *et al.* 2002), both regarded as characteristic of changes in solar forcing (Fig. 6). Low solar activity is associated with increased production of cosmogenic nuclides and is expected to induce climate deterioration (Stuiver *et al.* 1995; Grootes & Stuiver 1997). These authors suggested a solar origin for the weak Holocene (δ^{18}O-

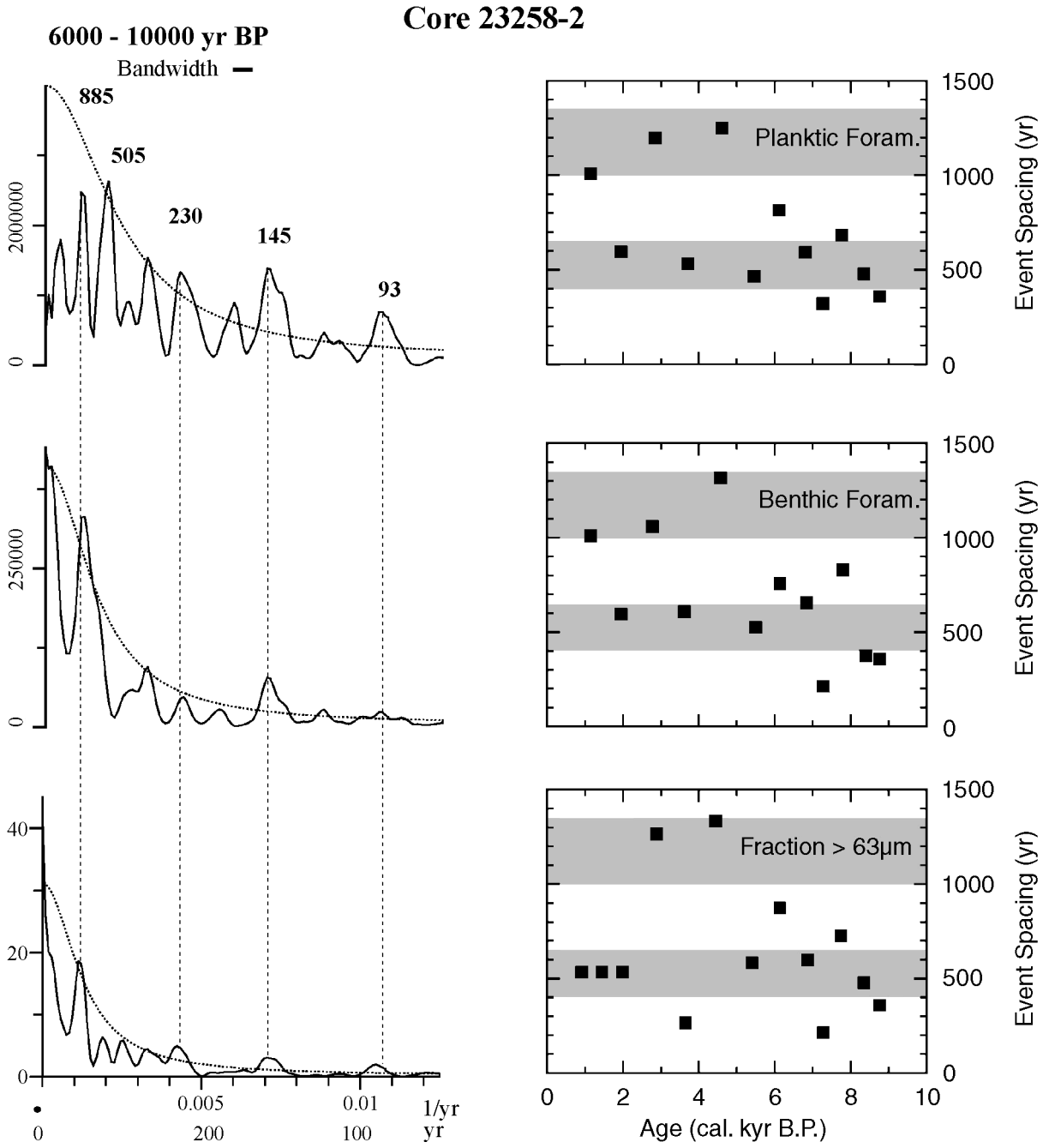

Fig. 5. Left panel: Power spectral density and salient periodicities of Early Holocene (10–6 kyr BP) sediment injections from the Barents shelf for core 23258-2 as indicated by maxima of planktic and benthic foraminifera tests and of sediment coarse fraction. Dotted 80% confidence line of red noise and spectra were estimated with the Redfit program (Schulz & Mudelsee 2002). Right panel: Temporal spacings of maxima in benthic and planktic foraminifera and coarse fraction over the entire Holocene as shown in Fig. 4. Grey bars delineate clusters of recurrence intervals.

based) climate cycles on Greenland on the basis of 510–530-year, (625-) and 830–1050-year-long oscillations in atmospheric ^{14}C content.

However, variations in oceanic THC may also lead to a differential transfer of CO_2 between the ocean and the atmosphere and thereby produce quasi-periodic changes in $\Delta^{14}C$ (i.e. of the atmospheric ^{14}C content). The THC linkage is supported by similar 550-year spectral peaks in $\Delta^{14}C$ and the $\%CaCO_3$ and planktic $\delta^{13}C$ records at North Atlantic Site NEAP15K, moreover, by the fact that the two signal groups are almost in phase (Chapman & Shackleton 2000).

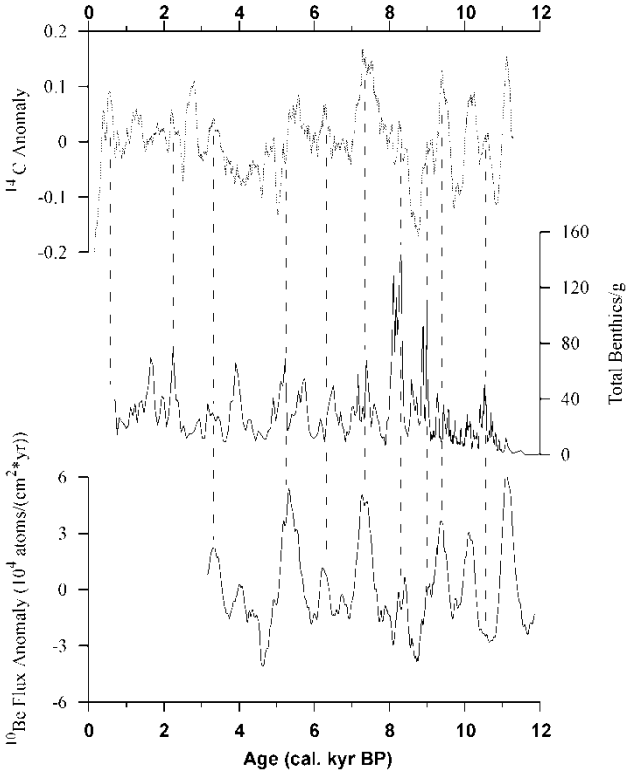

Fig. 6. Holocene variability of ^{14}C production rate and cosmogenic ^{10}Be as indicators of solar activity (Finkel & Nishiizumi 1997; Yiou *et al.* 1997; Bond *et al.* 2001; joint records provided by B. Kromer & J. Beer) versus changes in the abundance of benthic foraminifera, serving as indicator of lateral sediment injections from the Barents shelf. Solar proxies were detrended and smoothed (300-year running mean). Concomitant excursions of the records suggest solar climate forcing (tentatively marked by vertical lines). Non-coherent excursions may stem from uncertainties in the age model of core M23258.

Different from previous authors, Schulz & Paul (2002) succeeded in constraining more precisely the master periodicity in GISP2 δ^{18}O near 890 years for the early Holocene and 960 years for the entire Holocene (not shown), both numbers significant at 99.8%. On the one hand, this climate cycle may be linked to an orbital (eccentricity-linked) period which modulates incoming solar radiation (Loutre *et al.* 1992). On the other hand, the effect of this mode of orbital forcing on the Earth's climate is regarded as minor, since its maximum insolation changes hardly reach 1 mW m^{-2} at 65°N. Moreover, the two signals do not show a simple phase lock. Accordingly, Schulz & Paul (2002) assigned the millennial-scale changes in Holocene climate to the outlined internal oscillations of the ocean THC as ultimate forcing mechanism, similar to the Dansgaard-Oeschger cycles during MIS 2–4.

The temporal evolution of amplitudes in (1) the 890/960-year δ^{18}O signal at GISP2 and (2) the periodic sediment injections at Site 23258 differs significantly. In GISP2 the δ^{18}O amplitudes markedly decrease from early to late Holocene times (Schulz & Paul 2002), although the amplitude change may be overly dominated by the 8.3-kyr-cold event. In contrast, the amplitudes of the quasi-periodic sediment injections at Site 23258 remain approximately constant over the entire Holocene. This trend is similar to the major spikes of the Greenland ^{10}Be flux record (Figs 4, 6), which is mainly controlled by the atmospheric ^{10}Be concentration. Different from Δ^{14}C which may be also controlled by oceanic THC, the ^{10}Be flux is largely accepted as an unequivocal signal of changes in solar activity (Beer *et al.* 2002).

On the basis of Figs 5 and 6 we thus finally conclude (1) that the Holocene sediment injections from the western Barents shelf at Site 23258 reflect pulses of climate deterioration in northern high latitudes and (2) that their 400–650 and 1000–1350-year recurrence intervals may be paced by solar forcing (Fig. 6) on top of internal oscillations in the ocean THC. This conclusion is supported by the recent results of Bond *et al.* (2001), who also discussed the link between Holocene climate cycles and solar forcing on the basis of a coherency of 0.74 (significant at >95%) for ^{10}Be and stacked marine IRD records from the North Atlantic, although based on indistinct spectral peaks. The 1000–1350-year intervals are possibly multiples of the 400–650-year spacings.

In addition, the early Holocene frequency spectrum of sediment injections from the Barents shelf shows a number of significant periodicities near 230, 145 and 92/95 years (Fig. 5, left panel), well-known as Suess/deVries and Gleissberg cycles, driven by insolation changes (Beer *et al.* 1994; Hoyt & Schatten 1993; Stuiver *et al.* 1995; Yu & Ito 1999).

Obviously, the weak solar-induced climate variations are best recognized in Holocene climate records, where they are not concealed by other, stronger factors of millennial-scale climatic change, such as the DO cycles triggered by major ice breakouts from Greenland (as suggested by van Kreveld *et al.* 2000). They have predominated during cold marine isotope stages at lowered sea level only (Schulz *et al.* 1999) and, accordingly, have a much reduced influence on climate during Holocene times of high sea level, when ice breakouts are unlikely to occur along the East and North Greenland margins.

Conclusions

A Holocene sediment record from the lower western slope of the Barents shelf reveals some 13–15 distinct spikes of coarse sediment fraction, which equally consist of lithic grains and benthic and planktic foraminifera. The spikes are ascribed to lateral sediment injections produced by dense, highly turbid winter water cascades, such as monitored during modern winter. They result from enhanced sea ice formation and storminess on the

northern Barents shelf, i.e. from short-term pulses of climate deterioration, and reach down to the deep pycnocline near 1200 m water depth. Most prominent sediment injections mark the onset and end of the well-known cold spell 8300 years ago. The timing of sediment injections and storminess events closely resembles a storminess record from raised-beach ridges along the northern coastline of the Kola Peninsula.

The Early Holocene sediment injections from the Barents shelf show various significant and robust spectral peaks of 885 and 505 years. Over the entire Holocene, pervasive events recur every 400–650 and 1000–1350 years, similar to periodicities registered in the GISP2 $\delta^{18}O$ record, in $\Delta^{14}C$ and, most importantly, in the Greenland ^{10}Be flux (Stuiver *et al.* 1995; Chapman & Shackleton 2000; Schulz & Paul 2002). Accordingly, these Holocene periodicities are assigned to solar forcing, a weak climate factor only registered during the Holocene interglacial, when climatic change at multicentennial and millennial time scales was much less affected by strong thermohaline variations which produced the DO cycles characteristic of glacial times.

^{14}C datings in core 23258 in part were biased by the lateral admixture of old polar foraminifera from the Barents shelf. Thus the key to the age model was dating the subpolar species *N. pachyderma* (dex.), which only forms in the warm West Spitsbergen Current and cannot stem from lateral sediment injections. These dates helped to properly constrain the quality of the *N. pachyderma* (sin.) dates.

The major postglacial warming of the West Spitsbergen Current by 4–5°C is confined to the Early Holocene, 10.65–7.6 kyr BP. The timing of this early thermal maximum closely matches the thermal optimum found in ice cores from Severnaya Zemlaya and Greenland and a record of thermophilous molluscs on Spitsbergen, suggesting that this early thermal optimum was dominant over a broad region of the Eurasian Arctics. A cold spell intervened at 8.7–8.2 kyr (little prolonged by reworked polar foraminifera specimens). Most prominent temperature changes occurred within a few decades and less.

Acknowledgements. – We gratefully acknowledge the valuable help and suggestions of J. C. Duplessy, Gif-sur-Yvette and T. Kiefer, Kiel, and various colleagues in a joint EU project. B. Kromer, Heidelberg, and J. Beer, Bern, kindly provided updated versions of Holocene ^{14}C production rate and ^{10}Be flux. K. Kissling and several students assisted in producing the large data set with tedious but careful routine work. S. Rothe kindly helped with producing the final figures. This article benefited greatly from the constructive reviews of M. Hald, Tromsø and D. Lubinski, Boulder. The project was supported by EU contract ENV4-CT95-0131.

References

Alley, R. B., Ágústsdóttir, A.-M. & Fawcett, P. J. 1999: Ice-core evidence of late-Holocene reduction in North Atlantic ocean heat transport. *AGU Geophysical Monograph 112*, 301–312.

Backhaus, J. O., Fohrmann, H., Kämpf, J. & Rubino, A. 1997: Formation and export of water masses produced in Arctic shelf polynias process studies of oceanic convection. *ICES Journal of Marine Sciences 54*, 336–382.

Baldini, J. U. L., McDermott, F. & Fairchild, I. J. 2002: Structure of the 8200-year cold event revealed by a speleothem trace element record. *Science 296*, 2203–2206.

Bard, E., Arnold, M., Mangerud, J., Paterne, M., Labeyrie, L., Duprat, J., Milieres, M.-A., Sønstegaard, E. & Duplessy, J.-C. 1994: The North Atlantic atmosphere-sea surface ^{14}C gradient during the Younger Dryas climatic event. *Earth and Planetary Science Letters 126*, 275–287.

Bauch, H. A., Erlenkeuser, H., Spielhagen, R. F., Struck, U., Matthiessen, J., Thiede, J. & Heinemeier, J. 2001: A multiproxy reconstruction of the evolution of deep and surface waters in the Nordic Seas over the last 30,000 years. *Quaternary Science Reviews 20*, 659–678.

Beer, J., Baumgartner, S., Hannen-Dittrich, B., Hanenstein, J., Kubik, P., Lukasczyk, C., Mende, W., Stellmacher, R. & Suter, M. 1994: Solar variability traced by cosmogenic isotopes. *In* Pap, J. M., Fröhlich, C., Hudson, H. S. & Solanski, S. K. (eds.): *The Sun as a Variable Star: Solar and Stellar Irradiance Variations*, 291–300. Cambridge University Press, Cambridge.

Beer, J., Muscheler, R., Wagner, G., Laj, C., Kissel, C., Kubik, P. W. & Synal, H.-A. 2002: Cosmogenic nuclides during isotope stages 2 and 3. *Quaternary Science Reviews 21*, 1129–1140.

Bianchi, G. G. & McCave, I. N. 1999: Holocene periodicity in North Atlantic climate and deep-ocean flow south of Iceland. *Nature 397*, 515–517.

Blaume, F. 1992: Hochakkumulationsgebiete am norwegischen Kontinentalhang: Sedimentologische Abbilder topographiegeführter Strömungsmuster. *Berichte SFB 313, Universität Kiel 36*, 1–150.

Bond, G., Kromer, B., Beer, J., Muscheler, R., Evans, M. N., Showers, W., Hoffmann, S., Lotti-Bond, R., Hajdas, I. & Bonani, G. 2001: Persistent solar influence on North Atlantic Climate during the Holocene. *Science 294*, 2130–2136.

Bond, G., Showers, W., Cheseby, M., Lotti, R., Almasi, P., deMenocal, P., Priore, P., Cullen, H., Hajdas, I. & Bonani, G. 1997: A pervasive millennial-scale cycle in North Atlantic Holocene and glacial climates. *Science 278*, 1257–1266.

Bond, G., Showers, W., Elliot, M., Evans, M., Lotti, R., Hajdas, I., Bonani, G. & Johnson, S. 1999: The North Atlantic's 1–2 kyr climate rhythm: relation to Heinrich events, Dansgaard-Oeschger cycles and the Litte Ice Age. *AGU Geophysical Monograph 112*, 35–58.

Chapman, M. R. & Shackleton, N. J. 2000: Evidence of 550-year and 1000-year cyclicities in North Atlantic circulation patterns during the Holocene. *Holocene 10*, 287–291.

Dahl, S. O. & Nesje, A. 1996: A new approach to calculating Holocene winter precipitation by combining glacier equilibrium-line altitudes and pine-line limits: a case study from Hardangerjokulen, central southern Norway. *Holocene 6*, 381–398.

Dansgaard, W., Johnsen, S. J., Clausen, H. B., Dahl-Jensen, D., Gundestrup, N. S., Hammer, C. U., Hvidberg, C. S., Steffensen, J. P., Sveinbörnsdottir, A. E., Jouzel, J. & Bond, G. 1993: Evidence for general instability of past climate from a 250-kyr ice-core record. *Nature 364*, 218–220.

Denton, G. & Stuiver, M. 1969: Neoglacial chronology, northeastern Saint Elias Mountains, Canada. *In* Bushnell, V. C. & Ragle, R. H. (eds.): *Icefield Ranges Research Project Scientific Results*, *V. 1*, 173–186.

De Vernal, A., Hillaire-Marcel, C. & von Rad, U. 1997: Researchers look for links among paleoclimate events. *EOS 78*, 247, 249.

Digerfeldt, G. 1998: Reconstruction of Holocene lake-level changes in southern Sweden; techniques and results. *In* Harrison, S. P., Frenzel, B., Huckriede, U. & Weib, M. (eds.): Paleohydrology as reflected in lake-level changes as climatic evidence for Holocene times. *Palaeoklimaforschung 25*, 87–98G. Fischer Verlag, Stuttgart.

Duplessy, J.-C., Ivanowa, E., Murdmaa, I., Paterne, M. & Labeyrie, L. 2001: Holocene paleoceanography of the northern Barents Sea and variations of the northward heat transport by the Atlantic Ocean. *Boreas 30*, 2–16.

Finkel, R. C. & Nishiizumi, K. 1997: Beryllium 10 concentrations in the Greenland Ice Sheet Project 2 ice core from 3–40 ka. *Journal of Geophysical Research 102*, 26,699–26,706.

Fohrmann, H., Backhaus, J. O., Blaume, F., Haupt, B. J., Kämpf, J., Michels, K., Mienert, J., Posewang, J., Ritzrau, W., Rumohr, J., Weber, M. & Woodgate, R. 2001: Modern ocean current-controlled sediment transport in the Greenland–Iceland–Norwegian (GIN) Seas. *In* Schäfer, P., Ritzrau, W., Schlüter, M. & Thiede, J. (eds.): *The Northern North Atlantic: A Changing Environment*, 135–154. Springer-Verlag, Berlin.

Friedrich, M., Kromer, B., Spurk, M., Hofmann, J. & Kaiser, K. F. 1999: Palaeo-environmental and radiocarbon calibration as derived from Lateglacial / Early Holocene tree-ring chronologies. *Quaternary International 61*, 27–39.

Grootes, P. M. & Stuiver, M. 1997: Oxygen 18/16 variability in Greenland snow and ice with 10^{-3} to 10^{5}-year time resolution. *Journal of Geophysical Research 102*, 26,455–26,470.

Hald, M., Kolstad, V., Polyak, L., Forman, S. L., Herlihy, F. A., Ivanov, G. & Nescheretov, A. 1999: Late-glacial and Holocene paleoceanography and sedimentary environments in the St. Anna Trough, Eurasian Arctic ocean margin. *Palaeogeography, Palaeoclimatology, Palaeoecology 146*, 229–249.

Harrison, S. P. & Digerfeldt, G. 1993: European lakes as palaeohydrological and palaeoclimatic indicators. *Quaternary Science Reviews 12*, 233–248.

Hirschleber, H., Theilen, F., Balzer, W. & von Bodungen, B. 1988: Forschungsschiff Meteor, Reise 7: Berichte der Fahrtleiter. *Berichte SFB 313, Universität Kiel 10*, 1–257.

Honjo, S. 1990: Particle fluxes and modern sedimentation in the polar oceans. *In* Smith, W. O. Jr. (ed.): *Polar Oceanography. Part B: Chemistry, Biology, and Geology*, 687–739. Academic Press Inc, San Diego, CA.

Hoyt, D. V. & Schatten, K. H. 1993: A discussion of plausible solar irradiance variations 1700–1992. *Journal of Geophysical Research 98*, 18.895–18.906.

Huntley, B., Baillie, M., Grove, J. M., Hammer, C. U., Harrison, S. P., Jacomet, S., Jansen, E., Karlén, W., Koc, N., Luterbacher, J., Negendank, J. & Schibler, J. 2002: Holocene palaeoenvironmental changes in North-West Europe: climatic implications and human dimension. *In* Wefer, G., Berger, W. H., Behre, K.-E. & Jansen, E. (eds.): *Climate Development and History of the North Atlantic Realm*, 259–298. Springer-Verlag, Berlin.

Jensen, S. 1998: Planktische Foraminiferen im Europäischen Nordmeer: Verbreitung und Vertikalfluß sowie ihre Entwicklung während der letzten 15.000 Jahre. *Berichte SFB 313, Universität Kiel 57*, 1–105.

Johnsen, S. J., Dahl-Jensen, D., Gundestrup, N., Steffensen, J. P., Clausen, H. B., Miller, H., Masson-Delmotte, V., Sveinbjörnsdottir, A. E. & White, J. 2001: Oxygen isotope and palaeotemperature records from six Greenland ice-core stations: Camp Century, Dye-3, GRIP, GISP2, Renland, and North GRIP. *Journal of Quaternary Science 16*, 299–307.

Karlén, W. 1993: Glaciological, sedimentological and paleobotanical data indicating Holocene climatic change in northern Fennoscandia. *In* Frenzel, B., Eronen, M., Vorren, K. D. & Gläser, B. (eds.): *Oscillations of the Alpine and Polar Tree Limits in the Holocene*, 69–83. Gustav Fischer Verlag, Stuttgart.

Klitgaard-Kristensen, D., Sejrup, H. P. & Haflidason, H. 2001: The last 18 kyr fluctuations in Norwegian Sea surface conditions and implications for the magnitude of climatic change: evidence from the North Sea. *Paleoceanography 16*, 455–467.

Koç, N., Jansen, E. & Haflidason, H. 1993: Paleoceanographic reconstruction of surface ocean conditions in the Greenland, Iceland and Norwegian seas through the last 14 kyr based on diatoms. *Quaternary Science Reviews 12*, 115–140.

Koerner, R. M. & Fisher, D. A. 1990: A record of Holocene summer climate from a Canadian high-Arctic ice core. *Nature 343*, 630–631.

Korholla, A., Vasko, K., Toivonen, H. T. T. & Olander, H. 2002: Holocene temperature changes in northern Fennoscandia reconstructed from chironomids using Bayesian modelling. *Quaternary Science Reviews 21*, 1841–1860.

Labeyrie, L. D. & Duplessy, J. C. 1985: Changes in the oceanic $^{13}C/^{12}C$ ratio during the last 140,000 years: high-latitude surface water records. *Palaeogeography, Palaeoclimatology, Palaeoecology 50*, 217–240.

Loutre, M. F., Berger, A., Bretagnon, P. & Blanc, P.-L. 1992: Astronomical frequencies for climate research at the decadal to century time scale. *Climate Dynamics 7*, 181–194.

Lubinski, D. J., Forman, S. L. & Miller, G. H. 1999: Holocene glacier and climate fluctuations on Franz Josef Land, Arctic Russia, 80°N. *Quaternary Science Reviews 18*, 85–108.

Lubinski, D. J., Korsum, S., Polyak, L., Forman, S. L., Lehman, S. J., Herlihy, F. A. & Miller, G. H. 1996: The last deglaciation of the Franz Victoria Trough, northern Barents Sea. *Boreas 25*, 89–100.

Lubinski, D. J., Polyak, L. & Forman, S. L. 2001: Freshwater and Atlantic water inflows to the deep northern Barents and Kara seas since ca. 13 ^{14}C ka: foraminifera and stable isotopes. *Quaternary Science Reviews 20*, 1851–1879.

Malmgren, B. A., Kucera, M., Nyberg, J. & Waelbroeck, C. 2001: Comparison of statistical and artificial neural network techniques for estimating past sea surface temperatures from planktonic foraminifer census data. *Paleoceanography 16*, 520–530.

Malmgren, B. A. & Nordlund, U. 1997: Application of artificial neural networks to paleoceanographic data. *Palaeogeography, Palaeoclimatology, Palaeoecology 136*, 359–373.

Marchal, O., Cacho, I., Stocker, T. F., Grimalt, J. O., Calvo, E., Martrat, B., Shackleton, N. J., Vautravers, M., Cortijo, E., van Kreveld, S., Andersson, C., Koc, N., Chapman, M., Sbaffi, L., Duplessy, J. C., Sarnthein, M., Turon, J.-L., Duprat, J. & Jansen, E. 2002: Apparent long-term cooling of the surface in the northeast Atlantic and Mediterranean during the Holocene. *Quaternary Science Reviews 21*, 455–483.

Mayewski, P. A., Meeker, L. D., Twickler, M. S., Whitlow, S., Yang, Q., Lyons, W. B. & Prentice, M. 1997: Major features and forcing of high-latitude northern hemisphere atmospheric circulation using a 110,000-year-long glaciochemical series. *Journal of Geophysical Research 102*, 26,345–26,366.

McDermott, F., Mattey, D. P. & Hawkesworth, C. 2001: Centennial-scale Holocene climate variability revealed by a high-resolution speleothem $\delta^{18}O$ record from SW Ireland. *Science 294*, 1328–1331.

Midtun, L. 1985: Formation of dense bottom water in the Barents Sea. *Deep-Sea Research 32*, 1233–1241.

Møller, J. J., Yevzerov, V. Y., Kolka, V. V. & Corner, G. D. 2002: Holocene raised-beach ridges and sea-ice-pushed boulders on the Kola Peninsula, northwest Russia: indicators of climate change. *The Holocene 12*, 169–176.

Nadeau, M.-J., Schleicher, M., Grootes, P. M., Erlenkeuser, H., Gottdang, A., Mous, D. J. W., Sarnthein, J. M. & Willkomm, H. 1997: The Leibniz-Labor AMS facility at the Christian-Albrechts University, Kiel, Germany. *Nuclear Instruments and Methods in Physics Research B 123*, 22–30.

Patzelt, G. 1999: Werden und Vergehen der Gletscher und die nacheiszeitliche Klimaentwicklung in den Alpen. *Nova Acta Leopoldina NF 81*, 231–246.

Pflaumann, U., Duprat, J., Pujol, C. & Labeyrie, L. D. 1996: SIMMAX: a modern analog technique to deduce Atlantic sea surface temperatures from planktonic foraminifers in deep-sea sediments. *Paleoceanography 11*, 15–35.

Pflaumann, U., Sarnthein, M., Chapman, M., Funnell, B., Huels, M., Kiefer, T., Maslin, M., Schulz, H., Swallow, J., van Kreveld, S., Vautravers, M., Vogelsang, E. & Weinelt, M. In press: The glacial North Atlantic: sea surface conditions reconstructed by GLAMAP-2000. *Paleoceanography*.

Rumohr, J., Blaume, F., Erlenkeuser, H., Fohrmann, H., Hollender,

F.-J., Mienert, J. & Schäfer-Neth, D. 2001: Records and processes of near-bottom sediment transport along the Norwegian-Greenland sea margins during Holocene and late Weichselian (Termination I) times. *In* Schäfer, P., Ritzrau, W., Schlüter, M. & Thiede, J. (eds.): *The Northern North Atlantic: A Changing Environment*, 155–178. Springer-Verlag, Berlin.

Salvigsen, O., Forman, S. L. & Miller, G. H. 1992: Thermophilous molluscs on Svalbard during the Holocene and their paleoclimatic implications. *Polar Research 11*, 1–10.

Sarnthein, M., Jansen, E., Weinelt, M., Arnold, M., Duplessy, J.-C., Erlenkeuser, H., Flatoy, A., Johannessen, G., Johannessen, T., Jung, S., Koç, N., Labeyrie, L., Maslin, M., Pflaumann, U. & Schulz, H. 1995: Variations in Atlantic surface ocean paleoceanography, 50°–80°N: a time-slice record of the last 30,000 years. *Paleoceanography 10*, 1063–1094.

Sarnthein, M., Pflaumann, U., Vogelsang, E. & Weinelt, M. In press: Past extent of sea-ice in the northern North Atlantic inferred from foraminiferal paleotemperature estimates. *Paleoceanography*.

Schulz, M., Berger, W. H., Sarnthein, M. & Grootes, P. M. 1999: Amplitude variations of 1470-year climate oscillations during the last 100,000 years linked to fluctuations of continental ice mass. *Geophysical Research Letters 26*, 3385–3338.

Schulz, M. & Mudelsee, M. 2002: REDFIT: Estimating red-noise spectra directly from unevenly spaced paleoclimatic time series. *Computational Geoscience 28*, 421–426.

Schulz, M. & Paul, A. 2002: Holocene climate variability on centennial-to-millennial time scales: 1. Climate records from the North-Atlantic realm. *In* Wefer, G., Berger, W. H., Behre, K.-E. & Jansen, E. (eds.): *Climate Development and History of the North Atlantic Realm*, 41–54. Springer-Verlag, Berlin.

Simstich, J. 1999: Die ozeanische Deckschicht des Europäischen Nordmeers im Abbild stabiler Isotope von Kalkgehäusen unterschiedlicher Planktonforaminiferenarten. *Berichte – Reports, Institut für Geowissenschaften, Universität Kiel 2*, 1–96.

Simstich, J., Sarnthein, M. & Erlenkeuser, H. 2003: Paired $\delta^{18}O$ signals of *N. pachyderma* (s) and *T. quinqueloba* show thermal stratification structure in the Nordic Seas. *Marine Micropaleontology 48*, 107–125.

Stuiver, M., Grootes, P. M. & Braziunas, T. F. 1995: The GIPS2 $\delta^{18}O$ record of the past 16,500 years and the role of the sun, ocean and volcanoes. *Quaternary Research 44*, 341–354.

Stuiver, M., Reimer, P. J. & Braziunas, T. F. 1998: High-precision radiocarbon age calibration for terrestrial and marine samples. *Radiocarbon 40*, 1127–1152.

Thomsen, C., Blaume, F., Formann, H., Peeken, I. & Zeller, U. 2001: Particle transport processes at slope environments: event driven flux across the Barents Sea continental margin. *Marine Geology 175*, 237–250.

van Kreveld, S., Sarnthein, M., Erlenkeuser, H., Grootes, P., Jung, S., Nadeau, M. J., Pflaumann, U. & Voelker, A. 2000: Potential links between surging ice sheets, circulation changes, and the Dansgaard-Oeschger cycles in the Irminger Sea. *Paleoceanography 15*, 425–442.

Voelker, A. 1999: Dansgaard-Oeschger events in ultra-high resolution sediment records from the Nordic Seas. *Berichte – Reports, Institut für Geowissenschaften, Universität Kiel 9*, 1–278.

Vogelsang, E. 1990: Paläo-Ozeanographie des Europäischen Nordmeeres an Hand stabiler Kohlenstoff- und Sauerstoffisotope. *Berichte Sonderforschungsbereich 313, Universität Kiel 23*, 1–136.

von Bodungen, B., Bathmann, U., Voß, N. & Wunsch, M. 1991: Vertical particle flux in the Norwegian Sea: resuspension and interannual variability. *In* Wassmann, P., Heiskanen, A.-S. & Lindahl, O. (eds.): *Sediment Trap Studies in the Nordic Countries 2*, 116–136.

von Grafenstein, U., Erlenkeuser, H., Müller, J., Jouzel, J. & Johnsen, S. 1998: The cold event 8200 years ago documented in oxygen isotope records of precipitation in Europe and Greenland. *Climate Dynamics 14*, 73–81.

Wang, L., Sarnthein, M., Erlenkeuser, H., Grootes, P. M., Grimalt, J. O., Pelejero, C. & Linck, G. 1999: Holocene variations in Asian monsoon moisture: a bidecadal sediment record from the South China Sea. *Geophysical Research Letters 26*, 2889–2892.

Weinelt, M. 1993: Veränderungen der Oberflächenzirkulation im Europäischen Nordmeer während der letzten 60.000 Jahre – Hinweise aus stabilen Isotopen. *Berichte SFB 313, Universität Kiel 41*, 1–106.

Weinelt, M., Kuhnt, W., Sarnthein, M., Altenbach, A., Costello, O., Erlenkeuser, H., Pflaumann, U., Simstich, J., Struck, U., Thies, A., Trauth, M. & Vogelsang, E. 2001: Paleoceanographic proxies in the northern North Atlantic. *In* Schäfer, P., Ritzrau, W., Schlüter, M. & Thiede, J. (eds.): *The Northern North Atlantic: A Changing Environment*, 319–352. Springer-Verlag, Berlin.

Willemse, N. W. & Tørnquist, T. E. 1999: Holocene century-scale temperature variability from West Greenland lake records. *Geology 27*, 580–584.

Yiou, F., Raisbeck, G. M., Baumgartner, S., Beer, J., Hammer, C., Johnsen, S., Jouzel, J., Kubik, P. W., Lestringuez, J., Stiévenard, M., Suter, M. & Yiou, P. 1997: Beryllium 10 in the Greenland Ice Core Project ice core at summit, Greenland. *Journal of Geophysical Research 102*, 26,783–26,794.

Yu, Z. & Ito, E. 1999: Possible solar forcing of century-scale drought frequency in the northern Great Plains. *Geology 27*, 263–266.